Advances in Science and Technology Research Journal, 2026, 20(1), 222–235 https://doi.org/10.12913/22998624/211126 ISSN 2299-8624, License CC-BY 4.0

Received: 2025.08.06 Accepted: 2025.10.05 Published: 2025.11.21

Adverse effect on the strength and microstructural characteristics of iron-based binders under the influence of initial atmospheric exposure before CO₂ curing

Saranya Venkatachalam¹o, Karthiyaini Somasundaram¹*

- ¹ School of Civil Engineering, Vellore Institute of Technology, Chennai, India
- * Corresponding author's e-mail: karthiyaini.s@vit.ac.in

ABSTRACT

This study investigates the severe consequences of initial atmospheric exposure to iron-based alternative binders, focusing on the role of the addition of oxalic acid at various concentrations (0–4%) before the carbonation process. All iron-binder samples were subjected to 48 hours of pre-exposure to air, followed by 5 days of CO₂ curing after the initial hardening phase. Mechanical strength and microstructural analyses were performed to evaluate the performance and the reaction phases formed. The results revealed that the addition of oxalic acid to the iron binder contributed to the carbonation and iron dissolution processes even after atmospheric exposure. Microstructural analysis revealed the presence of siderite (FeCO₃) and calcite (CaCO₃), which contributed to denser matrix formation for strength gain. However, pre-exposure of already hardened samples to air led to non-uniform carbonation effects, where the outer surface carbonated, leaving the inner core of the samples resistant to CO₂ penetration, resulting in variation in strength. Overall, the study also validates the role of carbonation in the iron binder system, where the curing protocols adopted in this study show ineffective and nonuniform carbonation, providing negative consequences to carbon-cured construction materials.

Keywords: iron binder, oxalic acid, CO, curing, air exposure, mechanical properties.

INTRODUCTION

The global cement industry represents one of the most significant contributors to anthropogenic greenhouse gas emissions, constituting approximately 8% of the total CO, emissions worldwide, generating an estimated 4.1 billion tonnes of carbon dioxide annually [1]. This substantial environmental impact arises from dual emission sources, which involve the energy-intensive combustion processes required for clinker production at temperatures exceeding 1450 °C and the inherent chemical decomposition of limestone (CaCO₃ → CaO + CO₂) during calcination, which accounts for approximately 60% of cement-related emissions [2]. With global cement production projected to increase by 12-23% by 2050, driven by rapid urbanization and infrastructure development in emerging economies, the environmental implications of continued dependence on Portland cement have become increasingly unsustainable [3, 4].

Ferrock is an innovative iron-based binder that utilizes waste materials to produce a carbon-negative binding system through innovative carbonation chemistry. The study presented the carbonation of metallic iron powder with aqueous CO₂, along with additives (fly ash, limestone powder, metakaolin, and oxalic acid), to form complex iron carbonate binders [5-7]. The mechanical strength achieved was comparable to that of ordinary Portland cement (OPC). The carbon-negative potential of these is attributed to their unique carbonation mechanism, wherein atmospheric CO, reacts with iron particles under controlled humidity and pressure conditions to form iron carbonate phases, primarily siderite (FeCO₂), with minor phases including magnetite (Fe₃O₄) and various iron hydroxides [8, 9]. The complex carbonation process involved multiple consecutive reactions:

$$Fe^{2+} + CO_2 + H_2O \rightarrow FeCO_3 + H_2$$
 (primary carbonation) (1)

$$4Fe + 3O_2 + 6H_2O \rightarrow 4Fe (OH)_3$$
 (oxidation pathway) (2)

Fe
$$(OH)_3 + CO_2 \rightarrow FeCO_3 + H_2O + \frac{1}{2}O_2$$

(secondary carbonation) (3)

The formation of iron carbonate minerals in ferrock contributes directly to strength development and sequesters atmospheric carbon dioxide at rates of 0.5–1.5 kg CO₂ per kg, surpassing conventional concrete potential [10, 11]. The combined benefit mechanism distinguishes ferrock from conventional hydraulic cements that depend primarily on calcium silicate hydration reactions, and positions it as a carbon-negative construction application. Geopolymers utilize the alkali activation of aluminosilicate precursors and exhibit reduced reactivity to carbonation conditions compared with iron-based systems [12]. Magnesium oxychloride cement demonstrates rapid setting characteristics, but suffers from water sensitivity and limited durability in humid environments [13].

An early study [5] compared OPC with an iron-based binder, which achieved a strength of approximately 30 MPa, which is comparable to OPC systems. This study reported that the development of an iron-based binder is suitable for wider construction applications and is also benefits CO₂ sequestration [14]. The microstructural study revealed that the iron binder had refined pores during carbonation, leading to reduced porosity and enhanced densification [15]. Further examination of the iron carbonate binder temperature-induced systems confirmed the formation of stable siderite and other carbonate phases at elevated temperatures, highlighting the durability properties comparable to those of OPC [16, 17]. This study confirmed that iron-based concrete has better mechanical properties than equivalent curing periods, indicating a dense matrix formation of carbonate phases aligned with the performance and durability of OPC. Most literature on ferrock emphasizes the performance improvements for controlled carbonation conditions. Limited research has investigated how poor carbonation efficiency leads to failure pathways, and risk assessment remains insufficient. This knowledge gap presents

challenges for practical implementation, as ideal conditions are often difficult to achieve.

This study investigates the significant decrease of ineffective carbonation in ferrock through a comprehensive analysis of failure mechanisms induced by 48 hours of pre-air exposure followed by 5 days of CO, curing, which resulted in significant variation in strength development. This study involved various characterization approaches, including mechanical testing, microstructural analysis, and chemical composition evaluation, to demonstrate the degradation pathways associated with improper carbonation procedures. This investigation aims to establish essential control parameters for carbonation limits, detect governing failure mechanisms due to strength loss, and provide fundamental insights into the use of effective oxalic acid dosage variations to develop iron binders for carbon curing techniques. This study provides key insights into carbonation-related failure mechanisms and offers guidance for the development and application of alternative iron-based binders.

MATERIALS AND METHODS

The raw materials employed in this study included iron powder or steel dust, Class F fly ash, metakaolin, and calcium carbonate. The chemical compositions of the raw materials are listed in Table 1. Iron powder was sourced from Civitech Engineering Private Limited, and the remaining raw materials, metakaolin, calcium carbonate, and class F flyash, were purchased from Astra Chemicals, Chennai, India. In this study, the raw materials were combined with oxalic acid, which acts as a chelating agent, with a water-to-binder ratio (w/c) of 0.26. The mix proportions and sample specifications are presented in Table 2. The raw materials, iron powder, Class F fly ash, metakaolin, and calcium carbonate were first blended in a tray using a spatula to ensure the uniform distribution of the materials. Subsequently, oxalic acid and water were added to the dry blend to obtain a cohesive and homogeneous binder paste. The obtained iron-binder paste was blended using a mechanical mixer for 5 minutes to attain uniform consistency. After mixing, the paste was poured into a cubic mould measuring $50 \times 50 \times 50$ mm and prism moulds measuring $40 \times 40 \times 160$ mm. The step-by-step preparation, casting, and testing of iron binders are shown in Figure 1.

Table 1. Chemical composition of calcium carbonate, iron powder, metakaolin, and fly ash

| Raw materials | Chemical composition in % | | | | | | | | | | |
|-------------------|--------------------------------|--------------------------------|------|------------------|------------------|-------------------|-------------------------------|------|------------------|-----------------|--|
| | Fe ₂ O ₃ | Al ₂ O ₃ | CaO | K ₂ O | SiO ₂ | Na ₂ O | P ₂ O ₅ | MgO | TiO ₂ | SO ₃ | |
| Fly ash | 2.95 | 36.11 | 0.78 | 0.74 | 57.38 | - | 0.37 | 1.01 | 0.82 | 0.03 | |
| Iron powder | 87.32 | 0.33 | - | 0.01 | 1.32 | - | 0.34 | 0.15 | 0.00 | 0.18 | |
| Calcium carbonate | 3.27 | 35.95 | 2.01 | 0.27 | 43.74 | 0.11 | - | 0.68 | - | 0.07 | |
| Metakaolin | 0.54 | 46.70 | 0.09 | 0.12 | 50.20 | - | 0.39 | 0.17 | 1.47 | 0.03 | |

Table 2. Mix proportion of the iron-based binder

| MIX ID | Raw materials proportion in % | | | | | | | | | |
|----------|-------------------------------|---------|------------|-------------------|-------------|--------------|--|--|--|--|
| | Iron powder | Fly ash | Metakaolin | Calcium carbonate | Oxalic acid | Water/binder | | | | |
| Sample A | 60 | 20 | 8 | 8 | 4 | 0.26 | | | | |
| Sample B | 60 | 20 | 8 | 8 | 3 | 0.26 | | | | |
| Sample C | 60 | 20 | 8 | 8 | 2 | 0.26 | | | | |
| Sample D | 60 | 20 | 8 | 8 | 1 | 0.26 | | | | |
| Sample E | 60 | 20 | 8 | 8 | 0 | 0.26 | | | | |

Oxalic acid was added at various percentages of 0, 1, 2, 3, and 4, along with the raw materials and the required water. The oxalic acid content was limited to 4% as its solubility decreased beyond this level, with dissolution becoming less effective above 55 °C (376 g/L). The iron-binder paste was blended using a mechanical mixer for 5 minutes to achieve a uniform cohesion. After

mixing, the paste was poured into a cubic mould measuring $50 \times 50 \times 50$ mm and prism moulds measuring $40 \times 40 \times 160$ mm. Each sample ID was cast with 45 cubes and 15 prisms; three samples from each ID were tested at each age, and the average strength was reported for both compression and flexure. The samples were left to be exposed to air drying for 48 hours, and after



Figure 1. Preparation and testing of iron carbonate binder

demoulding, they were placed inside a carbonation chamber for CO, curing. The CO, chamber was maintained at a temperature of 30 ± 2 °C and relative humidity of $85 \pm 5\%$. CO₂ gas was introduced into the chamber at regular intervals to ensure saturation inside the chamber. Carbonation curing lasted up to 5 days, and later, the samples were tested for compressive strength at 7, 14, and 28 days. The flexural strength test was performed after 28 days. The compressive strength of the hardened cubes was evaluated using a Compression Testing Machine (CTM) with a maximum loading capacity of 2000 kN according to the ASTM C109 standard [18]. The prism samples were tested for flexural strength using a three-point loading machine at a loading speed of 0.1 mm/min, according to the ASTM C78 standard [19]. After testing, the samples were collected and their microstructural properties were analyzed using X-ray diffraction analysis (XRD) and scanning electron microscopy (SEM). XRD analysis was conducted to identify the crystalline phases present in the CO2-cured samples using an XRD RIGAKU SmartLab 3 kW apparatus in the range of 5 to 80. SEM analysis was performed using a Thermo Fisher FEI QUANTA 250 FEG instrument.

RESULTS AND DISCUSSION

Air-dried samples exposed to atmospheric conditions were tested for their compressive and flexural strength at different ages. These samples were then analyzed for microstructural characterization using scanning electron microscopy and X-Ray diffraction. The results are presented in Figures 1–6, and a detailed discussion was conducted to understand sample behaviour.

Compressive strength

The compressive strength of the iron-based binders incorporating varying percentages of oxalic acid in the cube samples was evaluated at 28 days, as depicted in Figure 2. The results revealed that there was a progressive strength gain over 28 days, confirming the carbonation reactions and formation of reaction products in the iron-based binders. Among the mixes, Sample A (4%) outperformed the other samples, whereas Sample B (3%) exhibited the lowest strength. The enhanced strength of sample A at 4% oxalic acid is attributed to the composition of iron powder, fly ash, limestone, and metakaolin. These compositions help enhance the overall reactivity and refine the

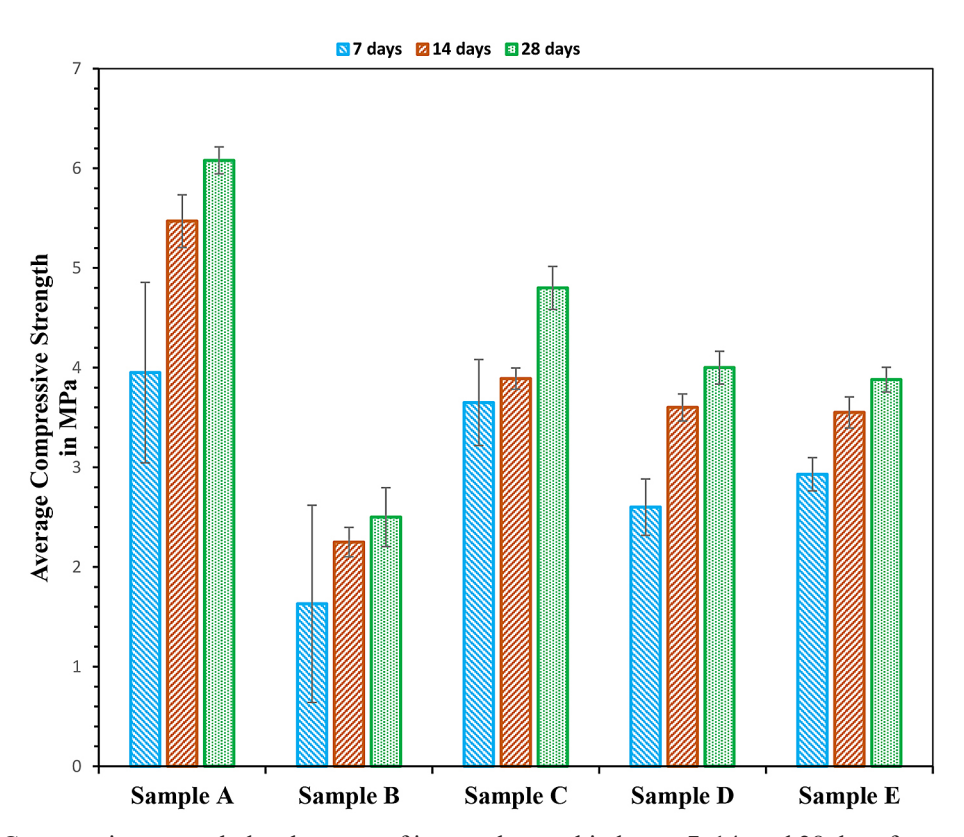


Figure 2. Compressive strength development of iron-carbonate binders at 7, 14, and 28 days for sample mixes with varying percentages of oxalic acid

microstructure by forming iron oxalates, contributing to a higher compressive strength [5, 20]. Iron oxalates precipitate into iron carbonate phases such as siderite (FeCO₃) [21]. This strength gain over time of carbonation is attributed to the densification of the microstructure induced by carbonation reactions and CO₂ diffusion into the matrix [22]. The iron carbonate formation reactions occurred when the samples were air-cured and cured in a CO₂ chamber. Carbonation reactions facilitated the early formation of iron phases such as Fe₂O₃ (hematite) and Fe₃O₄ (magnetite), which react with CO, to form stable iron carbonate (siderite) [23]. The lower strength of samples B and C (2–3%) indicated that the proportion of oxalic acid content influenced the carbonation kinetics, reduced the reaction kinetics, and formed fewer carbonate products [24]. The reduced formation of oxalates leads to insufficient chelation of iron ions, which slows the precipitation of the products [25]. Samples D (1%) and E (0%) performed better than sample B because of iron oxidation before the formation of the iron oxalate complexes. Sample E resulted in fewer carbonation reactions and lower strength due to the poor solubility and mobility of ions in the absence of oxalic acid.

This proves that the higher oxalic acid content (4%) promotes carbonation reactions with higher efficiency by facilitating ion mobility through chelation effects [26]. The chelating property of oxalic acid accelerates carbonation, forming carbonate phases at both early and long-term strengths [27]. The oxalic acid content enhanced the dissolution of iron and promoted denser matrix formation of the binder, with stable rhombohedral siderite crystals and calcite [15]. In contrast to lower oxalic acid dosages, the carbonation process is less efficient because of suboptimal chelating effects, which lead to incomplete carbonation reactions, limiting the formation of carbonate products and strength development [28]. The formation of surface precipitates due to CO2 exposure blocks further diffusion of CO₂, leading to various unreacted phases inside the matrix [29]. The dominant reaction mechanisms involved in the conversion of Fe to Fe²⁺ ions react with CO, molecules to form stable iron-carbonate complexes [30]. In the absence of oxalic acid, the insufficient mobility of the iron oxalate complexes hinders the carbonation reaction and the formation of carbonates. Initial air curing inhibited the oxidation reactions and ensured that the sample partially facilitated the formation of Fe₂O₂ and Fe₂O₄. Exposure of the sample to air allowed the oxidation

of iron, increasing its reactivity for subsequent carbonation. This results in immediate surface formation under CO_2 curing, which restricts further improvement of carbonation reaction kinetics. The combination of air curing and CO_2 curing maintained the reactivity of the binder, forming a less compact but sound carbonate matrix.

The standard deviation of the compressive strength results showed a relationship with the concentration of oxalic acid, particularly at an early age. At 7 days, samples with higher percentages of oxalic acid exhibited greater variability. Specifically, Sample B (3% oxalic acid) and Sample A (4% oxalic acid) had the highest standard deviations of 0.99 MPa and 0.91 MPa, respectively. In contrast, Sample E, which contained no oxalic acid, showed the most consistent results with the lowest standard deviation of 0.17 MPa. This suggests that the presence of oxalic acid, especially at higher concentrations, may introduce inconsistencies in the early strength development of ironbased binders. As the curing period progressed to 28 days, the variability generally decreased for most samples, with Sample E maintaining one of the lowest standard deviations at 0.12 MPa, indicating consistent long-term performance.

Flexural strength

The flexural strength results are shown in Figure 3. Sample A, with a higher flexural strength, suggests that the strength gain is due to the optimal formulation and microstructural development resulting from the enhanced reactivity and denser packing. The formation of siderite (FeCO₃), iron carbonate, and calcite (CaCO₃) phases contributes to the increased flexural strength [31]. The addition of oxalic acid acts as a chelating agent, which promotes ion mobility and denser matrix formation, favoring energy dissipation under loads [14]. From Figure 2. Sample B exhibited a lower strength than sample A (4%) and C (2%). This may be due to the over-chelation of oxalic acid and the immediate surface precipitation of Fe and Ca ions. The microstructure may form owing to inefficient carbonation, which causes the early failure of the sample [32]. Sample C performed well, indicating that oxalic acid improved matrix ductility and crack resistance under bending stress. This suggests that there is a balance between ion dissolution and carbonate precipitation, making the binder ductile [33]. In contrast, Samples B and D

show significantly lower strength owing to poor particle packing and incomplete carbonation reactions, which limit stress transfer during flexural loading [16]. In the case of sample D (1%), there was a slight decrease in the strength, indicating less carbonate formation and weaker internal bonding of the binder. A lower concentration of oxalic acid limits the availability of ions to participate in carbonation reactions, rendering the matrix fragile under bending [34]. Whereas Sample E (0%) attains lower flexural strength, in the absence of oxalic acid, there is poor ion dissolution and limited carbonate matrix formation. Air exposure alone is insufficient for the formation of crystalline phases to sustain stress. Partial air-drying leads to capillary stress, which forms micro-cracks, as these cracks act beneficially to provide nucleation sites during CO, curing. Initial oxidation leads to the formation of iron oxides before carbonation. Oxalic acid incorporation facilitates the chelation of Fe²⁺ and Ca²⁺ ions, increasing their solubility and denser matrix formation. This proves that there is a need for an ideal concentration of oxalic acid to perform carbonation reactions and produce carbonates [35]. The strength result indicates that the moderate strength gain is due to the partial development of carbonate phases in the reaction with iron phases and other reactive phases. At the same time, a lower percentage of oxalic acid leads to lower strength, which indicates that there are limited reactions in carbonation, which reduces the formation of carbonate phases [24, 36, 37].

According to previous studies on iron carbonate binder samples, these iron-based matrix

systems continue to densify over a long period due to the dissolution of Fe ions in the matrix and iron carbonate (FeCO₃) precipitation, which reduces the pore refinement and permeability. This indicates that the iron carbonate matrix is favorable in terms of durability against damage from moisture and carbonation-induced deterioration [15]. Furthermore, the presence of carbonate phases, such as siderite and calcite, along with unreacted Fe particles, enhances the stability of the material at high elevated temperatures, which improves the crack-bridging capacity and resistance to mechanical degradation [20].

For the 28-day flexural strength, the standard deviation did not follow a clear linear trend with respect to oxalic acid content. Sample B (3% oxalic acid) displayed the highest variability, with a standard deviation of 0.13 MPa. Conversely, Sample A, with the highest concentration of oxalic acid (4%), yielded the most consistent results, with the lowest standard deviation of just 0.05 MPa. The control mix, Sample E (0% oxalic acid), had a moderate standard deviation of 0.09 MPa. This pattern indicates that, while an intermediate concentration of 3% oxalic acid resulted in the least uniform flexural strength, the highest concentration of 4% produced the most consistent and reliable results among all the tested samples.

Overall, the mechanical strength (compression and flexure) depends more on the carbonate phase formation, along with other parameters, such as the homogeneity and integrity of the binder. Although oxalic acid, which is used as a chelating agent, catalyzes the reaction, the observation as a

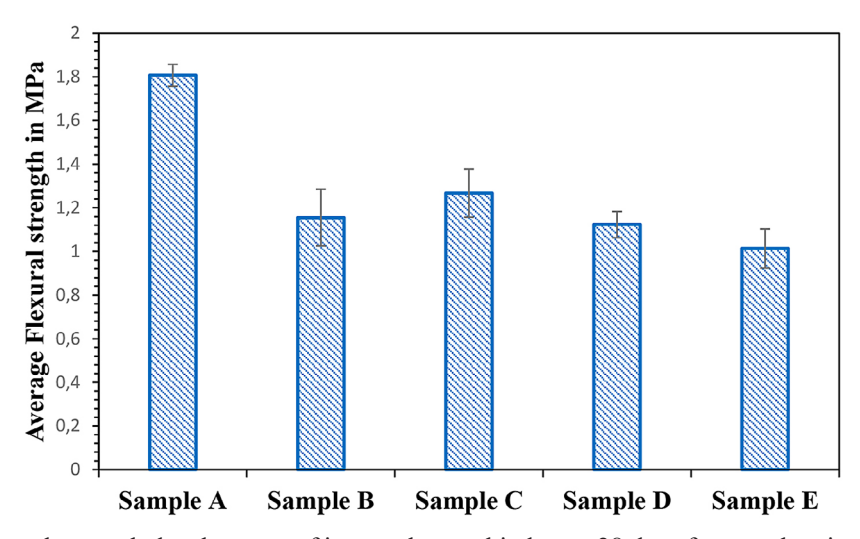


Figure 3. Flexural strength development of iron-carbonate binders at 28 days for sample mixes with varying percentages of oxalic acid

whole does not support the strength gain behavior owing to an increase in oxalic acid concentration. This shows that higher oxalic acid leads to a higher availability of free Fe ions, which are ready for carbonation. The strength depends solely on the rate of carbonation and the allowed carbonation period.

Scanning electron microscopy analysis

The microstructure and morphology of the reaction products in the iron-based binder system were examined using SEM to understand the reaction mechanism during carbonation curing. This study aimed to evaluate the impact of oxalic acid concentration on the carbonation efficiency, densification, and crystal formation in samples with different concentrations of oxalic acid: 4% (Figure 4) and 2% (Figure 5).

The 4% oxalic acid samples showed greater formation of siderite (Figure 4(A)). The siderite phases in carbonated systems occur when CO₂ dissolves in water and turns into carbonate ions (CO₃²). Siderite was observed as elongated, needle-shaped crystals that were slender in form [38]. The needle-like crystal morphology exhibits

a high nucleation density, as the iron surface rapidly becomes passivated because of the rapid precipitation of FeCO₃ from the atmosphere and the carbonation chamber [39]. The increased concentrations of Fe²⁺ and CO₃²⁻ ions accelerated the nucleation process, resulting in the production of elongated crystals, which were the carbonated phases in the iron carbonate binder. The observed crystal formation was due to the increased rate of ion exchange and the high surface area of the particles, which facilitated nucleation in certain regions of the iron particles.

The rhombohedral in shape, with well-formed FeCO₃ crystal structures, is seen in the iron carbonated binder SEM images in Figure 5(A), with 2% oxalic acid. A more balanced Fe²⁺/CO₃²⁻ ratio during precipitation typically leads to the formation of this crystal structure. This facilitated a more gradual nucleation and crystal growth process [40]. The outcome is larger, more systematically arranged crystals that can form a denser, more stable structure than needle-shaped varieties. This controlled formation indicates that the rates of CO₂ and iron dissolution can attain equilibrium, thereby promoting more organized and

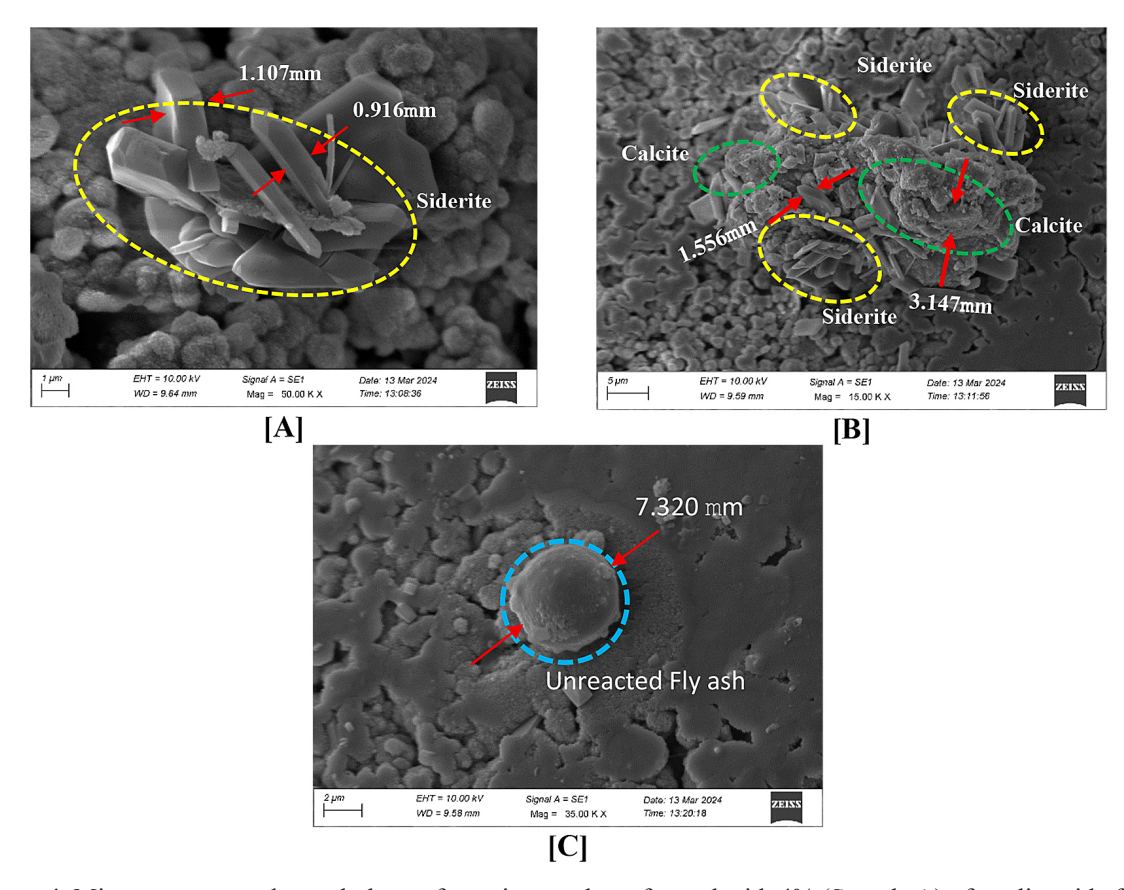


Figure 4. Microstructure and morphology of reaction products formed with 4% (Sample A) of oxalic acid after 2 days of air exposure and 5 days of CO₂ curing

robust crystal growth. This enhances the strength of the iron binder [41].

These shape modifications transformed not only the appearance of the carbonated products, but also the mechanical strength of the iron binder by promoting the growth of denser rhombohedron-shaped crystals, as shown in Figure 5(B). This improved bonding strengthened the material under strain [42]. The interplay among iron dissolution, carbon dioxide diffusion, and carbonate precipitation results in many pathways for crystal formation [43]. Under CO, curing conditions, a dense network of cementing particles developed. Conversely, if the conditions facilitate rapid nucleation with minimal growth, the resultant microstructure may exhibit numerous voids and insufficient carbonation, thereby weakening its structural integrity [44]. During carbonation, the interaction between Fe²⁺/Ca²⁺ ions and CO₂ molecules leads to the formation of rhombohedral siderite crystals (FeCO₂) and cubical calcite (CaCO₃) crystals [45]. The resulting shape from this process exhibited significant differences from that of pure siderite crystals, leading to a structure that was less compact and more porous.

Oxalic acid is a chelating chemical agent that helps iron particles dissociate into Fe²⁺ ions. Because of this reaction, more iron could react with CO, to produce FeCO₃, which is the major product of the iron carbonate binders [46]. The overall SEM examination showed that adding oxalic acid made the carbonated binder matrix denser and more compact. Calcite and siderite crystals spread out more uniformly in the matrix and have a higher density [44]. The compressive strength tests showed that this structure was more compact and uniform, which made the carbonated binder stronger [45]. The Fe-Ca systems of the deformed crystals show a higher porosity than the FeCO, compounds, which indicates the deterioration of the cementation properties of the system. In this process, the matrix of the iron binder reduces the strength because of the increased presence of pores and irregular crystal forms owing to improper binding. The samples with 2% oxalic acid showed greater formation of siderite, which led to a denser microstructure and increased the mechanical strength of the samples [46]. The unreacted fly ash in Figure 4(C) and Figure 5(C), which are shown in both oxalic acid percentages

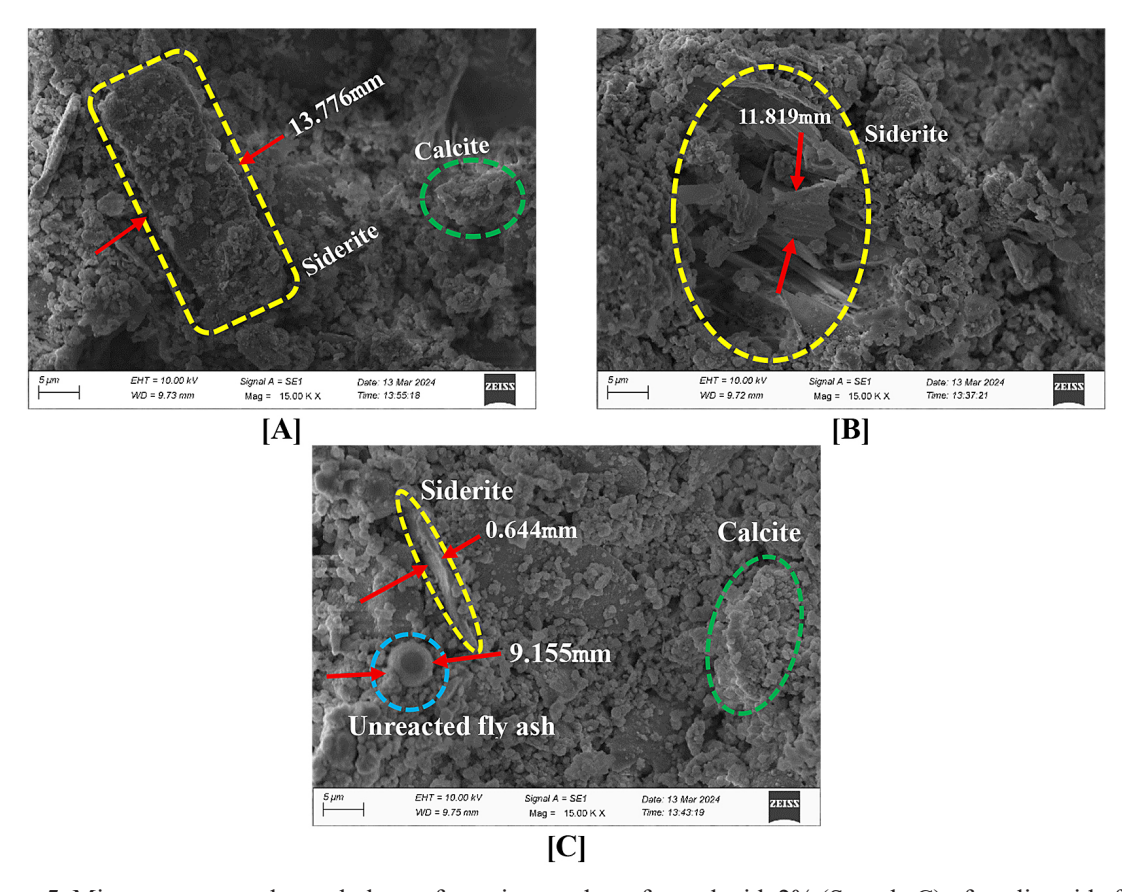


Figure 5. Microstructure and morphology of reaction products formed with 2% (Sample C) of oxalic acid after 2 days of air exposure and 5 days of CO₂ curing

of 2 and 4%, indicates that carbonation does not occur in this matrix, so the fly ash remains in the unreacted form.

The SEM analysis showed that the addition of 2% and 4% oxalic acid significantly enhanced the microstructure of the carbonated iron binders. Carbonated elements, such as granular CaCO₃ (calcite) and rhombohedral FeCO₃ (siderite), along with unreacted fly ash, increase the density of the matrix, indicating that these matrix systems exhibit better mechanical performance. The results indicate that blending oxalic acid with iron carbonation is an effective method for developing durable, viscous construction-based binders capable of sequestering CO₂.

X-ray diffraction analysis

The X-ray diffraction peaks of the carbonated iron-based binders containing 2% and 4% oxalic acid showed a composition of elements consisting of both reaction products and unreacted raw materials. The primary key components detected in the XRD analysis were siderite (FeCO₃), calcite (CaCO₃), magnetite (Fe₃O₄), alite (C₃S), quartz (SiO₂), and residual metallic iron (Fe). In addition, phase variations were observed in both the inner (core) and outer (surface) regions of the samples, as shown in Figures 6 and 7, respectively. A comparison of peak intensities and

distributions of peaks indicates that carbonation products form distinct peaks with different intensities of developed products due to varying levels of CO₂ exposure and ion exchange in the inner core and outer surface areas.

Siderite (FeCO₃)

The primary crystalline phase of siderite was observed in samples with 2% and 4% oxalic acid, as shown in Figures 6 and 7. The outer surface of the sample showed a strong and sharp peak in the 4% oxalic acid combination, indicating that siderite possessed a more crystalline structure and a higher volume fraction. The ability of oxalic acid to chelate facilitates the development of siderite by aiding the dissolution of Fe2+ ions from iron powder. In the aqueous phase, the dissolved iron readily interacts with CO2, resulting in the formation of siderite as a stable carbonate mineral [47]. A higher concentration of oxalic acid (4%) increases the availability of Fe2+, thereby accelerating the nucleation and formation of siderite crystals. These crystals exhibit strong adhesion properties in iron-based binders [48]. The inner core samples showed less intensity when compared to the outer samples of 4% oxalic acid because carbon dioxide diffusion was limited in the inner core samples; therefore, strong peaks of siderite formation were not observed in the inner core samples.

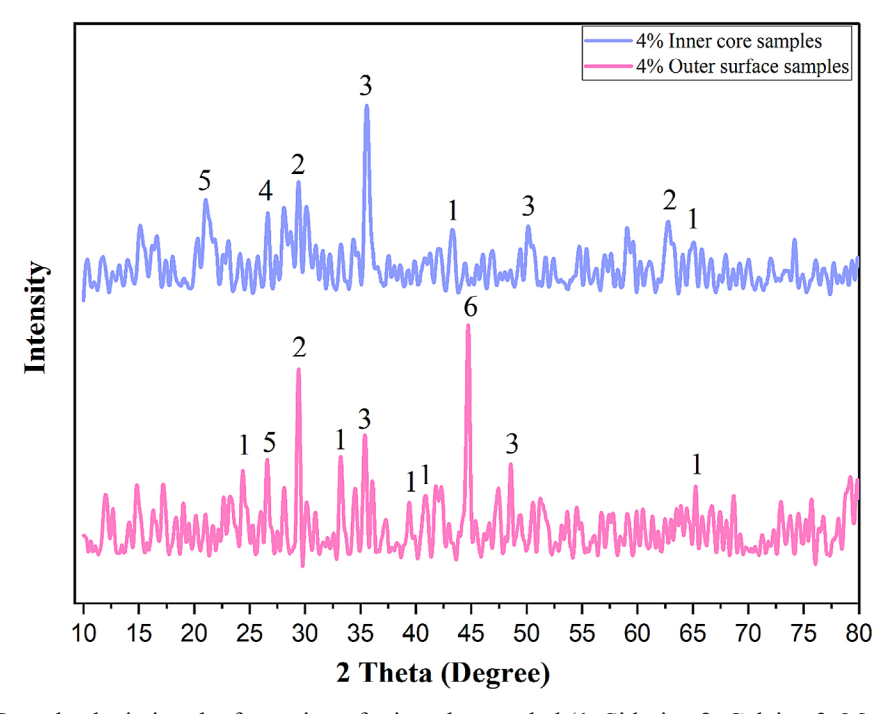


Figure 6. XRD peaks depicting the formation of minerals revealed (1. Siderite, 2. Calcite, 3. Magnetite, 4. Alite, 5. Quartz, and 6. Metallic iron) in the iron carbonate binder with 4% (Sample A) of oxalic acid

Calcite (CaCO₂)

The formation of calcite (CaCO₃) which is trigonal in shape, exhibited a pattern similar to that of siderite formation [49]. The outer layers showed stronger peaks at approximately 29.4°, particularly in the combination containing 4% oxalic acid. These peaks were observed in both oxalic acid samples, at 2% and 4%, but were stronger in the 4% sample. Because CO₂ availability was higher at the surface, this implies that Ca²⁺ ions, which were obtained from CaCO₃ and metakaolin, were more actively involved in carbonation at the surface of the samples [50]. The inner regions had lower calcite peaks, indicating a lower precipitation of CaCO₃. This is most likely due to the slower ion exchange and more difficult CO, diffusion. The combination of siderite and calcite formation in the matrix became denser and had fewer pores, which made the material tougher [51].

Magnetite (Fe,O,)

The inner core sample components of both samples with 2% and 4% oxalic acid exhibited a higher concentration of magnetite than the outer surface of the components. The intensity of the curves showed sharper and more pronounced peaks, particularly for the 2% oxalic acid sample. This indicates that the iron oxides did not completely

convert into carbonates in the inner core, because the reduced presence of chelating agents complicated the extraction of Fe²⁺ from Fe₃O₄, resulting in a significant amount of unreacted magnetite. Iron and carbon dioxide exhibit poor solubility owing to limited chelating activity and insufficient gas diffusion within the matrix [52]. In the external regions, the reduced magnetite intensity indicated a more effective transformation into siderite.

Alite (C,S – tricalcium silicate) and quartz (SiO,)

A quartz phase was observed in both regions and exhibited minimal variation in intensity, because it is an inert filler phase that does not participate in carbonation. However, alite, which is a hydraulic phase, was considerably more prevalent in the inner regions. This indicates that hydration is less probable because of the more intense carbonation reactions that occur at the surface. The outside region likely underwent initial carbonation, which limited the further hydration of alite [53]. The deficiency in hydration is possibly due to the reaction of CO₂ with dissolved Ca²⁺ and Fe²⁺ to form carbonates, which occur more frequently than the alite hydration pathways. The presence of quartz in both samples indicated that the silicaterich materials (fly ash and metakaolin) exhibited minimal alterations in their crystalline structures

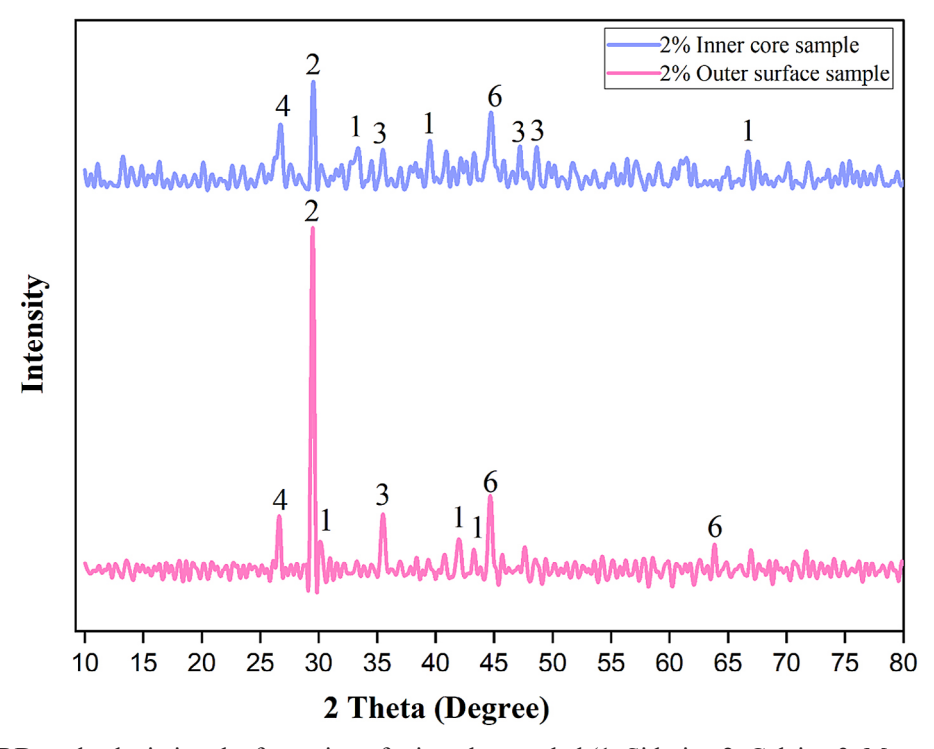


Figure 7. XRD peaks depicting the formation of minerals revealed (1. Siderite, 2. Calcite, 3. Magnetite, 4. Alite, 5. Quartz, and 6. Metallic iron) in the iron carbonate binder with 2% (Sample C) of oxalic acid

in the presence of carbon dioxide. Quartz primarily functions as a filler, enhancing the packing density and facilitating the mechanical interlocking of the matrix, although it does not directly participate in the carbonation reactions [54].

Metallic iron (Fe)

The peaks for unreacted iron at approximately 44.6° and 65° showed greater intensity in the inner core sample layers, particularly in the 2% oxalic acid sample. This indicates a higher presence of unconverted Fe owing to the lower reaction of oxalic acid and the poor penetration of CO₂ in the core. The outer surface of the samples showed reduced Fe peak intensities, indicating that iron dissolution and carbonate production were more distinct than those on the inner surface.

The variation in phase development between the inner core and outer layer samples of the binder matrix shows the significance of the carbon dioxide presence and oxalic acid percentage in controlling the carbonation process in the chamber [55]. In 2% oxalic acid, the chemical reactions of carbonation and dissolution were less efficient, especially in the inner core areas. The 4% oxalic acid samples exhibited improved carbonation efficiency and increased mechanical strength of the binder. The inner areas retained a greater amount of unreacted iron and magnetite, indicating that CO₂ diffusion was minimal and the carbonation reaction was reduced. The outer portion of the sample, which was directly exposed to carbon dioxide, resulted in the increased development of carbonated products such as calcite and siderite. This study was limited to 28 days of curing and up to a 4% range of oxalic acid concentrations, without long-term durability assessments. Future research should address extended curing, wider dosages, and durability aspects to validate the structural applicability.

The intensity of the peak of the 4 percent oxalic acid samples in Figure 6 is roughly proportional to the amount of the crystalline phase in the sample. The inner core sample shows magnetite (Fe₃O₄, peak 3) as the most intense peak in the pattern (at \sim 36° 2-theta), indicating that it is the most abundant crystalline component in the inner core. Calcite (CaCO₃, peak 2) at \sim 30° 2-theta was the second most intense. Calcite was a major component of the sample. Siderite (FeCO₃, peak 1), alite (Ca₃SiO₅, peak 4), and quartz (SiO₂, peak 5) show peaks of significantly lower intensity compared to

magnetite and calcite, suggesting they are present as minor components. Estimated abundance ranking (Inner Core): magnetite is greater than calcite and siderite. Outer surface sample shows a dramatic shift in composition where the metallic iron (Fe, peak 6) peak at $\sim 45^{\circ}$ 2-theta is exceptionally strong, dwarfing all other peaks. This indicated that metallic iron was the dominant crystalline phase on the surface. The calcite (CaCO₂, peak 2) peaks at ~30° 2-theta and remains strong, indicating that calcite is still a major component. Siderite (FeCO₃, peak 1), magnetite (Fe₃O₄, peak 3), and quartz (SiO₂, peak 5) were minor components. Notably, the intensity of the main magnetite peak (peak 3) decreased significantly compared with that of the inner core. The alite (Ca₃SiO₅, peak 4) phase was absent or below the detection limit, as its corresponding peak was missing. In general, this analysis revealed a clear chemical transformation. The process that occurred on the surface caused the reduction of the dominant magnetite phase in the core into metallic iron, which became the new dominant phase on the surface.

The intensity of the peak of the 2 percent oxalic acid samples in Figure 7 indicates an intense peak belonging to calcite (CaCO₂, peak 2), making it the most abundant crystalline phase. Alite (Ca, SiO₅, peak 4) also exhibited a strong peak, indicating that it was the second major component. The peaks for siderite (FeCO₃, peak 1), magnetite (Fe₃ O₄, peak 3), and metallic iron (Fe, peak 6) were present at significantly lower intensities. These are minor constituents of the core. The XRD pattern of the outer surface shows a dramatic change in the relative proportions of minerals. The peak for calcite (CaCO₂, peak 2) increased significantly in intensity, towering over all the other peaks. This signifies that calcite was the dominant crystalline phase on the sample surface. In comparison to the calcite peak, all other phases. Alite (Ca₃SiO₅, peak 4), siderite (FeCO₃, peak 1), magnetite (Fe₃O₄, peak 3), and metallic iron (Fe, peak 6) are present as minor or trace components. The relative intensity of the alite peak appears to have decreased compared with that of the inner core. The primary transformation from the inner core to the outer surface was a substantial increase in the relative amount of calcite. In general, the key quantitative difference was the significant enrichment of calcite on the outer surface, where it became the dominant phase. This is accompanied by a relative decrease in the proportion of alite.

CONCLUSIONS

The key findings of this study are to analyze the insights of carbonation during exposure to air and CO₂ curing for the development of iron-based alternative binders. This research highlights the following conclusions:

- 1. The formation of iron carbonate phases, such as FeCO₃ (siderite) and CaCO₃ (calcite), mainly contributes to strength development and stable matrix formation.
- The addition of oxalic acid promotes Fe ion dissolution and mobility through carbonation, resulting in a higher mechanical strength and denser microstructure.
- 3. An oxalic acid concentration of 4% is optimal for maximizing both the compressive and flexural strength of the iron-carbonate binder. This dosage proved superior to all other tested concentrations, including lower and intermediate amounts.
- 4. Oxalic acid acts as an effective chelating agent, accelerating the dissolution of iron (Fe²⁺ ions) and promoting the reaction with CO₂. This facilitates the formation of a dense, crystalline matrix of siderite (FeCO₃) and calcite (CaCO₃), which is the primary source of the binder's mechanical strength.
- 5. SEM confirmed the formation of siderite, calcite, and residual Fe with distinct morphologies linked to mechanical performance.
- 6. The inner core and outer surface in the XRD analysis demonstrate that there is variation in the distribution and intensity of the peaks due to reactivity and CO₂ exposure.
- 7. The study concluded that air exposure of the iron carbonate binder before CO₂ curing influenced the carbonation mechanism within the matrix.
- 8. The mechanical properties are a direct result of the binder's microstructure. The optimal 4% oxalic acid dosage creates a more compact and uniform matrix of carbonate crystals, leading to enhanced strength. In contrast, sub-optimal concentrations result in a less efficient, more porous structure that compromises performance.
- The partial oxidation that occurs during air exposure prior to carbonation leads to surface hardening, which restricts CO₂ penetration and reduces carbonation efficiency within the matrix.
- 10. The research was confined to a limited concentration range (up to 4%) and a short curing period of only 28 days. This prevents any conclusions about the long-term durability, potential degradation, or the effects of wider

dosage variations on the binder's performance in real-world structural applications.

Acknowledgment

The authors express their gratitude to Chandralega Viswanathan, Venkatesh Vellapandi, Shanmugasundaram Muthusamy and David Stone of Vellore Institute of Technology, Chennai, for their support in implementing this work. The authors acknowledge Civitech Engineering Private Limited for funding this project under CSR funding (Ref. No: CCSP2324039).

REFERENCES

- DiGiovanni C, Hisseine OA, Awolayo AN. Carbon dioxide sequestration through steel slag carbonation: Review of mechanisms, process parameters, and cleaner upcycling pathways. Journal of CO2 Utilization; 81. Epub ahead of print 1 March 2024. https://doi.org/10.1016/j.jcou.2024.102736
- Liu Q, Wang Y, Sun C, et al. Carbon sequestration and mechanical properties of foam concrete based on red mud pre-carbonation and CO₂ foam bubbles. Constr Build Mater; 426. Epub ahead of print 3 May 2024. https://doi.org/10.1016/j.conbuildmat.2024.135961
- 3. Hadi AM, Hasan KF, Ahmed IM, et al. Green Concrete: Ferrock Applicability and Cost-Benefit Effective Analysis, https://ejournal.bumipublikasinusantara.id/index.php/ajsem 2023.
- 4. Kaliyavaradhan SK, Ling TC. Potential of CO₂ sequestration through construction and demolition (C&D) waste An overview. Journal of CO₂ Utilization 2017; 20: 234–242.
- 5. Das S, Souliman B, Stone D, et al. Synthesis and properties of a novel structural binder utilizing the chemistry of iron carbonation. ACS Appl Mater Interfaces 2014; 6: 8295–8304.
- Vijayan DS, Dineshkumar, Arvindan S, et al. Evaluation of ferrock: A greener substitute to cement.
 In: Materials Today: Proceedings. Elsevier Ltd, 2020; 781–787.
- Veetil SP, Hitch M. Recent developments and challenges of aqueous mineral carbonation: a review. International Journal of Environmental Science and Technology 2020; 17: 4359–4380.
- Loder A, Siebenhofer M, Böhm A, et al. Clean iron production through direct reduction of mineral iron carbonate with low-grade hydrogen sources; the effect of reduction feed gas composition on product and exit gas composition. Clean Eng Technol; 5. Epub ahead of print 1 December 2021. https://doi.

- org/10.1016/j.clet.2021.100345
- Yuan S, Ding H, Wang R, et al. The mechanism of suspension reduction on Fe enrichment with lowgrade carbonate-containing iron ore. Advanced Powder Technology; 33. Epub ahead of print 1 July 2022. https://doi.org/10.1016/j.apt.2022.103643
- Niveditha M, Manjunath YM, Prasanna SHS. Ferrock: A carbon negative sustainable concrete. International Journal of Sustainable Construction Engineering and Technology 2020; 11: 90–98.
- 11. Feroz S, Krishna PVVSSR, Satyanarayana GVV, et al. Optimization of solids composition in ferrock mortar. In: E3S Web of Conferences. EDP Sciences, 2023. Epub ahead of print 5 June 2023. https://doi.org/10.1051/e3sconf/202339101218
- 12. Konduru H, Karthiyaini S, Shanmugasundaram M. Comparative study of silica fume and sodium silicate as replacement of active reactive silica in bauxite residue based geopolymer mortar. Case Studies in Construction Materials; 22. Epub ahead of print 1 July 2025. https://doi.org/10.1016/j.cscm.2025.e04302
- 13. Venkatesh V, Shanmugasundaram M. Enhancement of mechanical and microstructural characteristics of magnesium oxychloride cement with metasteatite. Case Studies in Construction Materials; 21. Epub ahead of print 1 December 2024. https://doi. org/10.1016/j.cscm.2024.e03683
- 14. Das S, Stone D, Convey D, et al. Pore- and microstructural characterization of a novel structural binder based on iron carbonation. Mater Charact 2014; 98: 168–179.
- 15. Das S, Stone D, Mobasher B, et al. Strain energy and process zone based fracture characterization of a novel iron carbonate binding material. Eng Fract Mech 2016; 156: 1–15.
- 16. Jeffy Pravitha J, Ninija Merina R, Subash N. Mechanical properties and microstructural characterization of ferrock as CO2–negative material in self-compacting concrete. Constr Build Mater; 396. Epub ahead of print 8 September 2023. https://doi.org/10.1016/j.conbuildmat.2023.132289
- 17. Luo Y, He D. Research status and future challenge for CO2 sequestration by mineral carbonation strategy using iron and steel slag. Environmental Science and Pollution Research 2021; 28: 49383–49409.
- 18. Standard Test Method for Compressive Strength of Hydraulic Cement Mortars (Using 2-in. or [50-mm] Cube Specimens) 1.
- Standard Test Method for Flexural Strength of Concrete (Using Simple Beam with Third-Point Loading) 1, www.astm.org
- 20. Das S, Kizilkanat AB, Chowdhury S, et al. Temperature-induced phase and microstructural transformations in a synthesized iron carbonate (siderite) complex. Mater Des 2016; 92: 189–199.

- 21. Lux S, Baldauf-Sommerbauer G, Ottitsch B, et al. Iron carbonate beneficiation through reductive calcination parameter optimization to maximize methane formation. Eur J Inorg Chem 2019; 2019: 1748–1758.
- 22. Bawab J, El-Hassan H, El-Dieb A, et al. Accelerated carbonation curing of concrete incorporating calcium carbide residue. Journal of Building Engineering; 88. Epub ahead of print 1 July 2024. https://doi.org/10.1016/j.jobe.2024.109258
- 23. Loder A, Siebenhofer M, Böhm A, et al. Clean iron production through direct reduction of mineral iron carbonate with low-grade hydrogen sources; the effect of reduction feed gas composition on product and exit gas composition. Clean Eng Technol; 5. Epub ahead of print 1 December 2021. https://doi. org/10.1016/j.clet.2021.100345
- 24. Ji L, Yu H, Zhang R, et al. Effects of fly ash properties on carbonation efficiency in CO₂ mineralisation. Fuel Processing Technology 2019; 188: 79–88.
- 25. Li L, Chen T, Gao X. Synergistic effect of CO2-mineralized steel slag and carbonation curing on cement paste. Cem Concr Compos; 145. Epub ahead of print 1 January 2024. https://doi.org/10.1016/j.cemconcomp.2023.105357
- 26. Lee SO, Tran T, Jung BH, et al. Dissolution of iron oxide using oxalic acid. Hydrometallurgy 2007; 87: 91–99.
- 27. Moon S, Kim E, Noh S, et al. Carbon mineralization of steel and iron-making slag: Paving the way for a sustainable and carbon-neutral future. J Environ Chem Eng 2024; 12: 112448.
- 28. Gu X, Wang S, Liu J, et al. Improving physical properties, microstructure and actual carbon sequestration of steel slag based autoclaved aerated concrete by accelerated carbonation. Journal of Building Engineering; 94. Epub ahead of print 1 October 2024. https://doi.org/10.1016/j.jobe.2024.110045
- Humbert PS, Castro-Gomes J. CO₂ activated steel slag-based materials: A review. Journal of Cleaner Production 2019; 208: 448–457.
- Qu Y, Xing L, Shao L, et al. Microstructural characterization and gas-solid reduction kinetics of iron ore fines at high temperature. Powder Technol 2019; 355: 26–36.
- 31. Kusin FM, Hasan SNMS, Molahid VLM, et al. Carbon dioxide sequestration of iron ore mining waste under low-reaction condition of a direct mineral carbonation process. Environmental Science and Pollution Research 2023; 30: 22188–22210.
- 32. Srivastava S, Snellings R, Meynen V, et al. Siderite-calcite (FeCO₃–CaCO₃) series cement formation by accelerated carbonation of CO₂(g)–H₂O–Fe–Ca(OH)2 systems. Cem Concr Compos; 122. Epub ahead of print 1 September 2021. https://doi.org/10.1016/j.cemconcomp.2021.104137
- 33. Das S, Hendrix A, Stone D, et al. Flexural fracture

- response of a novel iron carbonate matrix Glass fiber composite and its comparison to Portland cement-based composites. Constr Build Mater 2015; 93: 360–370.
- 34. Nayak S, Krishnan NMA, Das S. Fracture response of metallic particulate-reinforced cementitious composites: Insights from experiments and multiscale numerical simulations. Cem Concr Compos 2019; 97: 154–165.
- 35. Davoodi S, Al-Shargabi M, Wood DA, et al. Review of technological progress in carbon dioxide capture, storage, and utilization. Gas Science and Engineering; 117. Epub ahead of print 1 September 2023. https://doi.org/10.1016/j.jgsce.2023.205070
- 36. Ma Z, Liao H, Wang L, et al. Effects of iron/silicon/magnesium/aluminum on CaO carbonation of CO₂ in steel slag-based building materials during carbonation curing. Constr Build Mater; 298. Epub ahead of print 6 September 2021. https://doi.org/10.1016/j.conbuildmat.2021.123889
- Ahmad S, Assaggaf RA, Maslehuddin M, et al. Effects of carbonation pressure and duration on strength evolution of concrete subjected to accelerated carbonation curing. Constr Build Mater 2017; 136: 565–573.
- 38. Srivastava S, Snellings R, Meynen V, et al. Utilising the principles of FeCO3 scaling for cementation in H₂O-CO₂(g)-Fe system. Corros Sci; 169. Epub ahead of print 1 June 2020. https://doi.org/10.1016/j. corsci.2020.108613
- Roelands CPM, Ter Horst JH, Kramer HJM, et al. Analysis of nucleation rate measurements in precipitation processes. Cryst Growth Des 2006; 6: 1380–1392.
- 40. Li Y, Xin H, Zong Y, et al. A novel nucleation-induced crystallization process towards simultaneous removal of hardness and organics. Sep Purif Technol; 307. Epub ahead of print 15 February 2023. https://doi.org/10.1016/j.seppur.2022.122785
- 41. Norouzpour M, Santos RM, Chiang YW. Activation methods for enhancing CO₂ mineralization via mine tailings—A critical review. Carbon Capture Science and Technology; 15. Epub ahead of print 1 June 2025. https://doi.org/10.1016/j.ccst.2025.100430
- 42. Liendo F, Arduino M, Deorsola FA, et al. Factors controlling and influencing polymorphism, morphology and size of calcium carbonate synthesized through the carbonation route: A review. Powder Technology; 398. Epub ahead of print 1 January 2022. https://doi.org/10.1016/j.powtec.2021.117050
- 43. Barker R, Burkle D, Charpentier T, et al. A review of iron carbonate (FeCO₃) formation in the oil and gas industry. Corrosion Science 2018; 142: 312–341.
- 44. Shi X, Zhang C, Gupta KK, et al. Risks of cement and rock-cement-metal interface degradation in geological carbon sequestration reservoirs:

- Mechanisms, influencing factors and mitigation measures. Carbon Capture Science and Technology; 15. Epub ahead of print 1 June 2025. https://doi.org/10.1016/j.ccst.2025.100419
- 45. Somani RS, Patel KS, Mehta AR, et al. Examination of the polymorphs and particle size of calcium carbonate precipitated using still effluent (i.e., CaCl₂ + NaCl solution) of soda ash manufacturing process. Ind Eng Chem Res 2006; 45: 5223–5230.
- 46. Liu F, Peng C, Wilson BP, et al. Oxalic acid recovery from high iron oxalate waste solution by a combination of ultrasound-assisted conversion and cooling crystallization. ACS Sustain Chem Eng 2019; 7: 17372–17378.
- 47. Li R, Zhang T, Liu Y, et al. Calcification-carbonation method for red mud processing. J Hazard Mater 2016; 316: 94–101.
- 48. Saran RK, Arora V, Yadav S. Co2 sequestration by mineral carbonation: A review. Global Nest Journal 2018; 20: 497–503.
- 49. Zavarzina DG, Kochetkova T V., Chistyakova NI, et al. Siderite-based anaerobic iron cycle driven by autotrophic thermophilic microbial consortium. Sci Rep; 10. Epub ahead of print 1 December 2020. https://doi.org/10.1038/s41598-020-78605-7
- 50. Saranya V, Karthiyaini S, Stone D. Enhancement of strength and microstructural characterization in red mud-iron carbonate binders: Effects of CO₂ sequestration and oxalic acid concentration. Results in Engineering 2025; 25: 104539.
- 51. Santawaja P, Kudo S, Mori A, et al. Sustainable ironmaking using oxalic acid: the concept, a brief review of key reactions, and an experimental demonstration of the iron-making process. ACS Sustain Chem Eng 2020; 8: 13292–13301.
- 52. Nouar SL, Djebaili Baki A, Iddou A. Studies of the mechanism of poly (vinyl alcohol) (PVA) adsorption on the calcite/water interface in the presence of sodium oleate (SOL). Res J Chem Environ 2007; 11: 52–62.
- 53. Cisiński M, Biava G, Winnefeld F, et al. Carbonated calcium silicates as pozzolanic supplementary cementitious materials. Constr Build Mater; 443. Epub ahead of print 13 September 2024. https://doi.org/10.1016/j.conbuildmat.2024.137764
- 54. Chandralega V, Shanmugasundaram M, Stone D. Enhancing the performance of iron-based binders with seawater and CO₂ sequestration. Case Studies in Construction Materials 2025; 22: e04367.
- 55. de Jesus Andrade Fidelis R, Pires M, de Resende DS, et al. Magnetite: Properties and applications A review. Journal of Magnetism and Magnetic Materials; 614. Epub ahead of print 15 February 2025. https://doi.org/10.1016/j.jmmm.2025.172770